

Thermal, Structural and Magnetic Properties Study of $Zn_{0.85}Mg_{0.15}Fe_2O_4$ Nanomagnetic Material

Gishu Semu Telila

Department of Physics, College of Natural Science, Arba Minch University, Arba Minch, Ethiopia

Abstract - $Zn_{0.85}Mg_{0.15}Fe_2O_4$ nanomagnetic material was synthesized by solid state reaction method at a temperature of $800^\circ C$ using high pure metal oxide raw materials. Thermogravimetric analysis (TGA)-differential thermal analysis (DTA), powder x-ray diffraction (XRD), Fourier transform infrared (FT-IR) spectroscopy, electron spin resonance (ESR) spectroscopy characterization techniques were utilized to investigate the thermal, the structural and magnetic properties of the synthesized sample. The total weight loss regions were identified from TGA-DTA analysis. The XRD and FT-IR analysis revealed the formation of cubic spinel structure with $Fd-3m$ space group nanosized material. XRD measurement also showed that the synthesized material in the form of powder has an average crystal size of 20 nm. From the ESR spectroscopy investigation, wide line width and large g -value were identified. The large value of Lande's g parameter revealed the dominance of the dipolar interactions in $Zn_{0.85}Mg_{0.15}Fe_2O_4$ ferrite particles.

Keywords: Solid state reaction method; Characterization; Thermal property; Structure; Magnetic property.

1. INTRODUCTION

Ferrites are magnetic compounds which are composed of metallic oxides and iron oxide as their main components. Most of ferrites have spinel structure with a formulae AB_2O_4 , where "A" are divalent ions such as Ni^{2+} , Cu^{2+} , Co^{2+} , Cd^{2+} , etc. and "B" are the trivalent ions such as Fe^{3+} , Cr^{4+} and Al^{3+} [1]. In recent years, spinel ferrites have been investigated because of their great useful electrical and magnetic properties as well as their wide applications, such as microwave devices, magnetic switches, electromagnetic circuits, magnetic cores, medical diagnostics, information storage etc. [2]. These properties of ferrites depend on several factors, such as synthesis method, the distribution of cations along the tetrahedral and octahedral sites, calcination as well as sintering conditions, chemical composition, crystal size and cation distribution in the two sub-lattices [2,3]. Moreover, these properties of spinel ferrite can be controlled by chemical composition, substitution, method of synthesis and the particle size.

Therefore, serious studies have been carried out to improve the magnetic and electrical properties of ferrites. Ferrites are very known magnetic materials widely used in different technological applications [1,2]. They have a structure with a formula AB_2O_4 , where "A" are divalent cations such as Cu^{2+} , Co^{2+} , Cd^{2+} , Ni^{2+} , Zn^{2+} and "B" are trivalent cations such as Co^{3+} , Al^{3+} , Fe^{3+} [3,4]. Depending on the cation occupancy, spinel ferrites are basically classified into normal, mixed and inverse ferrites. In normal spinel, the divalent cations "A" are positioned at the tetrahedral sites and the trivalent cations "B" on the octahedral sites. In mixed spinel structure, both divalent and trivalent cations occupy both the tetrahedral and octahedral sites. In an inverse spinel, "A" cation occupies one half of the octahedral coordination sites and half the "B" cation occupies the other half octahedral sites as well as all tetrahedral sites. For instance, $NiFe_2O_4$ has an inverse spinel crystal structure [4,5]. Thus, Ni cations occupy half of the octahedral coordination sites and Fe cations occupy the remaining half octahedral sites as well as all tetrahedral sites. The unit cell of spinel ferrites contains 32 oxygen atoms in cubic close packing with 8 tetrahedral and 16 octahedral occupied sites. In recent years, nanocrystalline ferrites have attracted much interest because of their unique magnetic properties and their promising technological applications. These ferrites are materials of interest because of their unique electric, dielectric and magnetic properties. They are also very important group of magnetic materials due to their extensive use in a wide range of applications from low to high permeability devices including electronics, ferrofluid, magnetic drug delivery microwave devices, and high density information storage devices [6-10].

Spinel $ZnFe_2O_4$ ferrite has received broad interest in various fields, because of its unique physical and chemical properties. It has also very wide technological applications, such as drug delivery technology and magnetic resonance imaging (MRI) and photocatalysis [11-14]. The bulk $ZnFe_2O_4$ has a normal spinel structure with Zn^{2+} ions are preferentially occupied the tetrahedral (A) sites and the octahedral [B] sites are occupied by Fe^{3+} ions. However, the cation distribution in tetrahedral and octahedral sites depends on the particle size and the synthesis method [14].

It has also been reported that the reduction of the particle size can induce the formation of partially inverse spinel structure with novel magnetic properties such as net magnetic moment and ferromagnetism at room temperature [15–18]. Different authors reported that the physical properties of $ZnFe_2O_4$ can be improved by the substitution of the divalent or trivalent magnetic or diamagnetic cations [19–22].

$ZnFe_2O_4$ ferrite has been synthesized by various methods such as solid-state reaction, sol-gel, hydrothermal, co-precipitation, combustion techniques [23-25]. Solid state synthesis method is mostly utilized to prepare $ZnFe_2O_4$ based ferrites materials due to its simplicity in synthesis procedure, low-cost and suitability for mass-production. In this study, solid state synthesis method was chosen for the synthesis of $Zn_{0.85}Mg_{0.15}Fe_2O_4$ ferrite. TGA-DTA, XRD, FT-IR spectroscopy, ESRS were employed to study the thermal, structural and magnetic properties of this ferrite material.

2. MATERIALS AND METHODS

2.1. Synthesis Procedures

Mg cation substituted $ZnFe_2O_4$ nanomagnetic material with a chemical formula $Zn_{0.85}Mg_{0.15}Fe_2O_4$ was synthesized by solid state reaction method using high pure Zinc Oxide (ZnO), Ferric Oxide (Fe_2O_3), Magnesium Oxide (MgO) starting materials. Stoichiometric amount of the ZnO , MgO and Fe_2O_3 raw materials was initially mixed together and well grounded into a fine powder using agate mortar and pestle for about two hours. Further, about four milliliters amount of methanol was added to into the mixture for homogenizing the mixture and grounded for an hour. The obtained powder material was calcined in air at a temperature of $800^\circ C$ for 12 hours in controllable furnace with $5^\circ C/min$ for both heating and cooling. The calcined powder was finally crushed in an agate mortar to obtain the final product.

2.2. Material Characterizations

Thermal analysis of the sample was conducted using simultaneous DTA-TGA thermal analyzer apparatus (DTG-60H) instrument. For this purpose, about 14.74 mg sample was used and this sample was heated from room temperature to $1000^\circ C$ in the TGA furnace at a heating and cooling rate of $10^\circ C$ per min in nitrogen atmosphere. The crystal structure of the resulting $Cu_{0.8}Zn_{0.2}Fe_2O_4$ material in the form of powder was identified by XRD using a Phillips XPERT-PRO diffractometer using $Cu\ K\alpha$ radiation ($\lambda = 1.54060\ \text{\AA}$). The diffraction pattern was recorded in angular range between diffraction angles $2\theta = 20^\circ$ and 80° . The infrared spectrum was obtained in the transmittance

method with potassium Bromide (KBr) as IR window in the wave number region of $400 - 1,500\ cm^{-1}$ using ALFA-T instrument. The room temperature magnetic measurement of the prepared sample was carried out with electron spin resonance spectroscopy using JEOL model FA100 instrument. The external magnetic field was applied in the range of 50 to 500 mT.

3. RESULTS AND DISCUSSION

3.1. Thermal Analysis

Thermal analysis study of $Zn_{0.85}Mg_{0.15}Fe_2O_4$ sample was conducted by heating 14.74 mg of the mixture of ZnO , MgO and Fe_2O_3 precursors before the calcination process in the temperature range of $15^\circ C$ to $1000^\circ C$. The obtained TGA-DTA curves are shown in figure 1. As it can be seen in the figure, the thermal decomposition of the precursors takes place in different stages. The significant weight loss regions as well as the stable phase formation region are also identified. In the present investigation, the first weight loss region in the temperature range of $22 - 212^\circ C$ is 0.5 mg or 2.94% is due to the loss of adsorbed water. This effect is also identified by a sharp endothermic peak centered at around $83.5^\circ C$. The second stage of TGA curve shows weight loss of 1.5 mg or 8.81% between the temperature of 212 and $518.5^\circ C$. This loss is associated with the decomposition of the oxide precursors to form $Zn_{0.85}Mg_{0.15}Fe_2O_4$ compound. The decomposition reaction is depicted as a sharp endothermic peak in the DTA curve centered at $297^\circ C$. The

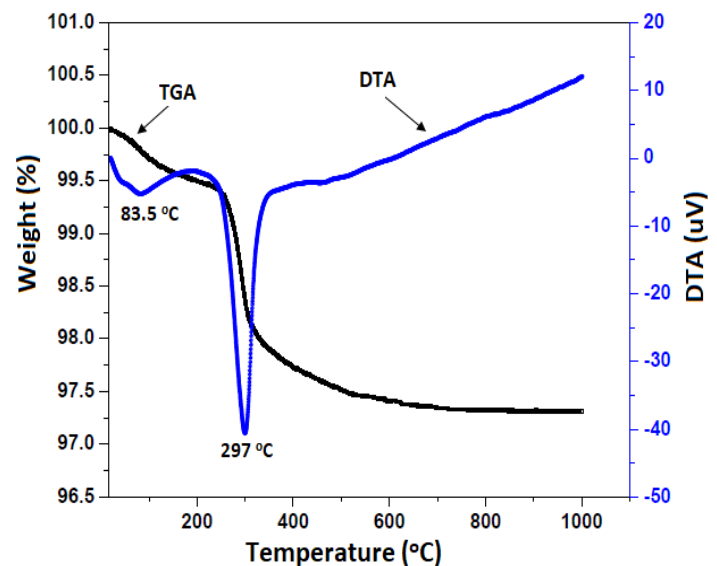


Figure-1: TGA/DTA curves of $Zn_{0.85}Mg_{0.15}Fe_2O_4$ ferrite material.

third weight loss observed in the temperature range of 518.5 and 1000 °C is 0.67 mg or 3.95 %. This loss is associated with the decomposition of the remaining raw materials. At higher temperatures, the TGA curve becomes more flattened, indicating stable phase formation of $Zn_{0.85}Mg_{0.15}Fe_2O_4$ ferrite material. In the DTA curve, the observed endothermic peaks are related to the weight loss stages in the TGA profile. So, they are characteristic of energy changes corresponding to different weight losses. Above 458°C, the gradual shift of the base line indicates that the solid-state reaction to form a pure phase $Zn_{0.85}Mg_{0.15}Fe_2O_4$ ferrite material.

3.2. XRD Study

The phase formation of $Zn_{0.85}Mg_{0.15}Fe_2O_4$ powder sample was detected by using X-ray diffraction technique in the range of 2θ between 20° and 80° after the sample is calcined at $800^\circ C$ for 12 hours. The obtained XRD pattern is shown in figure 2. As it is observed in the figure, the obtained diffraction patterns clearly show that all the peaks are sharp and well-defined, indicates that the synthesized sample possesses good degree of crystallinity. The XRD pattern of the sample also show considerable broadening of the peaks, which is indicates the particles of the synthesized samples are in nanometer range [26]. Moreover, the synthesized sample shows the characteristic peaks of ferrite material with most intense peak (311), which confirms the formation of cubic spinel structure. The peaks at 2θ values corresponding to 18.6° , 30.1° , 35.2° , 36.9° , 43.0° , 56.8° , 62.5° , 70.8° , 73.8° and 77.5° can be indexed to (111), (220), (311), (222), (400), (511), (440), (620), (533) and (622) crystal planes respectively. This indicates the formation of spinel cubic structure with $Fd3m$ space group, which is in accordance with the phases of $ZnFe_2O_4$ (JCPDS: PDF no. 74-2397, $Fd-3m$ (227)). However, additional peaks are observed in these XRD patterns demonstrating the presence of other phase besides the $Zn_{0.85}Mg_{0.15}Fe_2O_4$ ferrite structure. These have been attributed to the following impurities Fe_2O_3 and F_3O_4 in addition to ZnO and MgO.

The lattice parameter (a) of $Zn_{0.85}Mg_{0.15}Fe_2O_4$ ferrite material was calculated by the least square fitting method from the d-spacing and the Miller indices, hkl using following relation;

$$a = d\sqrt{h^2 + k^2 + l^2} \quad (1)$$

The average crystallite size (D) of this sample was calculated using Scherrer's formula [26];

$$D = \frac{0.9\lambda}{\beta \cos \theta} \quad (2)$$

where λ is the X-ray wavelength, θ is the Bragg diffraction angle of (311) plane, and β is the full width half maxima (FWHM). The lattice constant and the crystal size of the sample was calculated by indexing the XRD patterns at (400) and X-ray peak broadening of the (311) peak, respectively.

The unite cell volume (V) of the synthesized sample was also calculated by;

$$V = a^3 \quad (3)$$

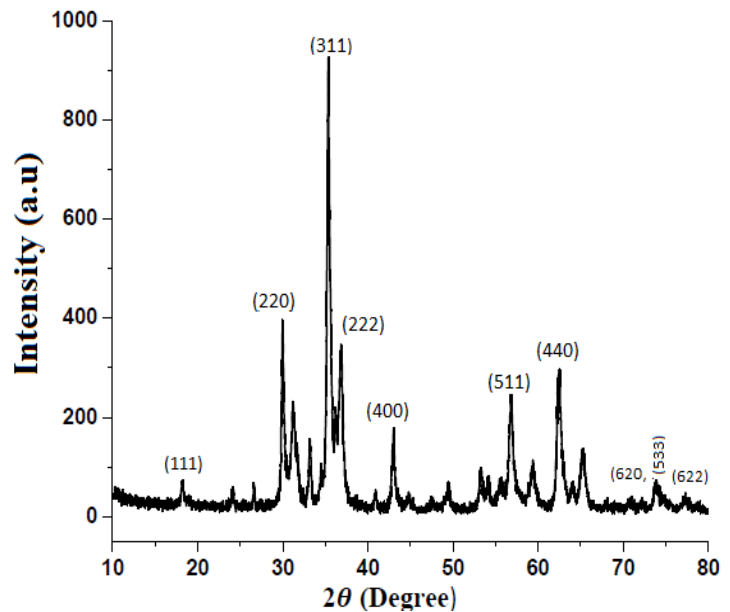


Figure-2: XRD pattern of $Zn_{0.85}Mg_{0.15}Fe_2O_4$ ferrite material.

The obtained results are shown in Table 1. As it observed in the table the lattice parameter, the unite cell volume and the crystal size of $Zn_{0.85}Mg_{0.15}Fe_2O_4$ are found to be 8.409 \AA , $594.61 (\text{ \AA})^3$ and 20 nm , respectively. The obtained crystallite size confirms the nano crystalline nature of the $Zn_{0.85}Mg_{0.15}Fe_2O_4$ ferrite material. On the other hand, the calculated lattice parameter of $Zn_{0.85}Mg_{0.15}Fe_2O_4$ ferrite sample is slightly lower when compared with the pure $ZnFe_2O_4$ (8.443 \AA) [27], which is associated with the ionic radius of Mg^{2+} ion (0.65 \AA) is lower than that of Zn^{2+} ions (0.83 \AA) [27]. The decrease in the unite cell volume of the sample is attributed to the increase in its lattice constant. Similar report has been made by Manikandan et al. [27].

3.3. FT-IR analysis

The FT-IR analysis study is an important method to get information about the positions of the ions in the crystal through the crystal's vibrational modes. In the previous

Table - 1: 2θ values, d-spacing, lattice constants, cell volumes and crystal sizes of $Zn_{0.85}Mg_{0.15}Fe_2O_4$ ferrite material.

Sample	2θ value for (400) (degree)	d-spacing for (400) (Å)	Lattice Constant a (Å)	Unit Cell Volume V (Å) ³	Crystal Size from (311) (nm)
$Zn_{0.85}Mg_{0.15}Fe_2O_4$	42.9897	2.10225	8.409	594.61	20

studies it is reported that the formation of $ZnFe_2O_4$ ferrite can be identified by FT-IR spectra through the existence of characteristic vibrational bands of the tetrahedral (A) and octahedral (B) sites. The difference in positions of the bands for the various compositions of ferrite materials was expected because of the difference in the distances for the octahedral and tetrahedral ions. It is also reported that the vibrational spectra of ferrite materials attribute the band around 600 cm^{-1} to the intrinsic vibrations of tetrahedral sites and around 400 cm^{-1} to that of octahedral sites [28,29]. According to Patil [28], ν_1 band corresponds to the stretching vibrations of Zn^{2+} -O band in tetrahedral sites, while ν_2 is assigned to Fe^{3+} -O stretching of octahedral sites. This formation of bands verifies the formation of spinel $ZnFe_2O_4$ compound.

In this study, the FT-IR spectrum of $Zn_{0.85}Mg_{0.15}Fe_2O_4$ ferrite sample is shown in figure 2. As observed in the figure, the FT-IR spectrum shows two distinct absorption bands which are responsible for the formation $Zn_{0.85}Mg_{0.15}Fe_2O_4$ compound. The higher frequency band (ν_1) is located at

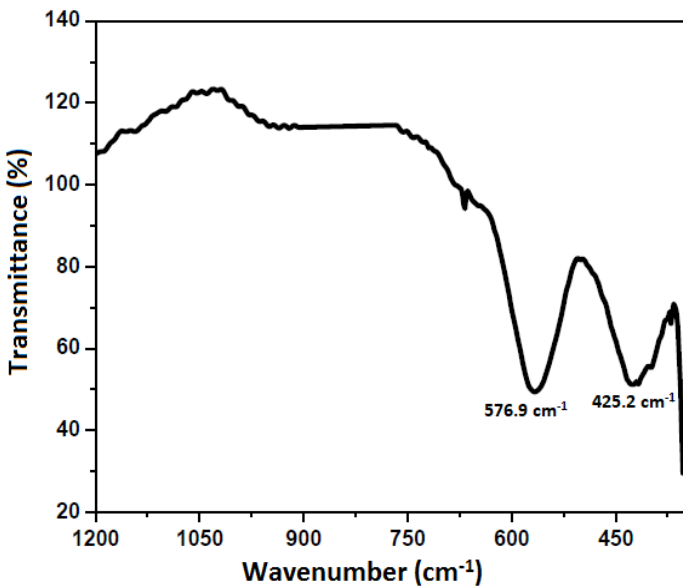


Figure - 3. FT-IR spectra of $Zn_{0.85}Mg_{0.15}Fe_2O_4$ ferrite material.

576.9 cm^{-1} and the lower frequency band (ν_2) is located at 425.2 cm^{-1} . The band with peak at 576.9 cm^{-1} may be associated with the stretching vibration of the $Zn(Mg)$ -O bonding force in $Zn_{0.85}Mg_{0.15}Fe_2O_4$ ferrite. Similarly, the band with peak at 425.2 cm^{-1} may also be associated with the stretching vibration of the Fe -O bonding force in $Zn_{0.85}Mg_{0.15}Fe_2O_4$ ferrite. The difference in frequency bands ν_1 and ν_2 may be attributed to the changes in bond lengths between metal-oxygen ions within octahedral and tetrahedral sites. As compared with the bands of $ZnFe_2O_4$ compound reported by Konicki et al. [30], the absorption peak of $Zn_{0.85}Mg_{0.15}Fe_2O_4$ ferrite is shifted slightly towards higher wavenumber region. This change in band position may be due to the substitution of Mg^{2+} ions for Zn^{2+} ions leads to the decrease in metal-oxygen separation. This is also in good agreement with the lower lattice parameter, unit cell volume and crystal size calculated from the XRD pattern.

The force constant for tetrahedral site (K_t) and octahedral site (K_o) were calculated using the relation [31];

$$K_t = 7.62 \times M_1 \times \nu_1^2 \times 10^{-7} \text{ N/m} \quad (4)$$

$$K_o = 10.62 \times \frac{M_2}{2} \times \nu_2^2 \times 10^{-7} \text{ N/m} \quad (5)$$

where M_1 and M_2 are the molecular weights of cations at tetrahedral and octahedral sites, respectively, and ν_1 & ν_2 are the frequency bands at tetrahedral and octahedral sites, respectively. The elastic force constants for tetrahedral site (K_t) of $Zn_{0.85}Mg_{0.15}Fe_2O_4$ compound is found to be 1.5×10^4 dyne/cm. Further, the elastic force constants for octahedral site (K_o) of $Zn_{0.85}Mg_{0.15}Fe_2O_4$ compound is found to be 0.77×10^4 dyne/cm. As compared both obtained results, the calculated values of K_T is larger than that of K_o . However, the tetrahedral bond length values of both ferrites are lower than those of octahedral site, which is associated with the shorter bond length of tetrahedral cluster and longer bond length of octahedral cluster [31].

3.4. ESR Spectroscopy Study

In electron spin resonance (ESR) study, the position of the ESR signal depend on the ratio of the magnetic field to magnetic field frequency and the effective gyromagnetic factor (g-factor). From the width and shape of the resonant

lines, it is possible to obtain detailed information about the magnetic nature of different materials. The ESR spectrum for $Zn_{0.85}Mg_{0.15}Fe_2O_4$ ferrite was recorded at a constant microwave frequency of 9450 MHz in the presence of a magnetic field of 650 mT. The effective g factor of the synthesized sample was evaluated using the relation [32];

$$g = \frac{h\nu}{\mu_B H_r} \quad (6)$$

where ν is frequency of electromagnetic radiation, h is Planck's constant (1.054×10^{-34} J-s), μ_B is Bohr magneton (9.274×10^{-24} J/T), H_r is resonance field. The resonance line width ΔH_{pp} is defined as peak-to-peak distance of the ESR signal. In this study, the room temperature the ESR study of $Zn_{0.85}Mg_{0.15}Fe_2O_4$ ferrite which was prepared by solid state reaction method at calcination temperature of 800°C is shown in Figure 4. The calculated values of resonance field H_r , peak to peak line width and Lande's g-factor are shown in Table 2.

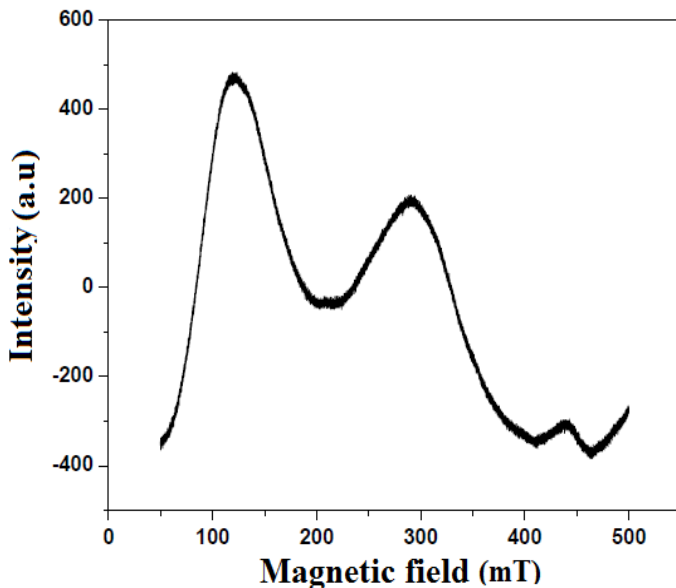


Figure-4. ESR spectra for $Zn_{0.85}Mg_{0.15}Fe_2O_4$ ferrite.

As observed from the figure, the ESR spectrum of the synthesized sample shows a relatively broadened signal with line width ΔH_{pp} 169.5 mT and 3.35 effective g values. Here, the obtained g value of the sample is relatively large. This may be a characteristic of isolated Fe^{3+} ions predominantly situated in the $Zn_{0.85}Mg_{0.15}Fe_2O_4$ crystal lattice. This confirms the presence of Fe_2O_3 impurity. Different research studies reported that the ESR signal for ferrite materials generally originated from magnetic dipole interactions among particles and super exchange interactions between magnetic ions through oxygen ions [33]. The line width of ESR signal may get broadened or

narrowed depending upon the interaction inside the ferrite material. Dominant dipole interactions give rise to broadened line width and large value of g-factor [34]. From the ESR spectroscopy investigation, wide line width and large g-values are obtained, which indicates that dipole interactions are dominant in $Zn_{0.85}Mg_{0.15}Fe_2O_4$ ferrite particles. From the ESR study small resonance peaks are observed in the range 385.7 mT to 484.9 mT. This may be associate with the presence of impurities in the prepared sample.

Table – 2: ESR parameters of the synthesized material.

Compound	Peak to peak line width (mT)	Resonance field (mT)	g-value
$Zn_{0.85}Mg_{0.15}Fe_2O_4$	169.5	209.4	3.35

4. CONCLUSIONS

Nanomagnetic $Zn_{0.85}Mg_{0.15}Fe_2O_4$ material was successively prepared by a solid-state reaction method using ZnO, MgO and Fe_2O_3 precursors. The thermal property, structural and magnetic properties of the synthesized material were investigated. It was found that the obtained nanomagnetic material possessed a spinel types cubic structure with Fd-3m space group. The FT-IR absorption bands within the frequency range supported the formation of the cubic structure in $Zn_{0.85}Mg_{0.15}Fe_2O_4$ compound. The XRD measurement showed that the lattice parameter as well as the crystal size of the synthesized nanocrystalline were found to be about 8.409 Å and 20 nm, respectively. These values were lower than those reported by other researchers for $ZnFe_2O_4$. From XRD study, the presence of additional impurities in synthesized sample was identified. These impurities caused a crucial role in the magnetic behavior of the sample. The room temperature ESR spectroscopy confirmed the dominance of the dipole interactions in $Zn_{0.85}Mg_{0.15}Fe_2O_4$ ferrite particles.

ACKNOWLEDGEMENT

The author is gratefully acknowledged to Dr. Paulos Taddesse for his support and guidance. The author also expresses his sincere thanks to Dr. Vijaya Babu for the FT-IR as well as ESR characterization and Adama Science and Technology University for XRD and TGA-DTA characterization.

REFERENCES

- [1]. M.T. Rahman, M. Vargas, C.V. Ramana, Structural Characteristics, Electrical Conduction and Dielectric

- Properties of Gadolinium Substituted Cobalt Ferrite. *Journal of Alloys and Compounds*, *Journal of Alloys and Compounds*, vv. 617, 2014, pp. 547–562.
- [2]. G. Mustafa, M.U. Islam, W. Zhang, Y. Jamil, A.W. Anwar, M. Hussain, M. Ahmad, Investigation of Structural and Magnetic Properties of Ce³⁺-Substituted Nanosized Co-Cr Ferrites for a Variety of Applications, *Journal of Alloys and Compounds*, vv. 618, 201, pp. 428–436.
- [3]. M.D.P. Silva, F.C. Silva, F.S.M. Sinfrônio, A.R. Paschoal, E.N. Silva, C.W.A. Paschoal, The effect of cobalt substitution in crystal structure and vibrational modes of CuFe₂O₄ powders obtained by polymeric precursor method, *Journal of Alloys and Compounds*, vv. 584, 2014, pp. 573–580.
- [4]. Nicola A. Spaldin, *Magnetic Materials: Fundamentals and Applications*, second ed., Cambridge University Press, Cambridge, 2010.
- [5]. I. Nlebedim, N. Ranvah, P. Williams, Y. Melikhov, F. Anayi, J. Snyder, A. Moses, D. Jiles, Influence of vacuum sintering on microstructure and magnetic properties of magnetostrictive cobalt ferrite, *Journal of Magnetism and Magnetic Materials*. Vv. 321, 2009, pp. 2528–2532.
- [6]. Y. Qu, H. Yang, N. Yang, Y. Fan, H. Zhu and G. T. Zou, The Effect of Reaction Temperature on the Particle Size, Structure and Magnetic Properties of Coprecipitated CoFe₂O₄ Nanoparticles, *Materials Letters*, vv. 60, 2006, pp. 3548–3552.
- [7]. P. L. Phillips, J. C. Knight, B. J. Mangan, P. St. J. Russell, M. D. B. Charlton and G. J. Parker, Near-Field Optical Microscopy of Thin Photonic Crystal Films, *Journal of Applied Physics*, vv. 85, 1999, pp. 6338–6345.
- [8]. M. H. Sousa and F. A. Tourinho, New Electric Double-Layered Magnetic Fluids Based on Copper, Nickel, and Zinc Ferrite Nanostructures, *Journal of Physical Chemistry B*, vv. 105, 2001, pp. 1168–1175.
- [9]. F. Mazaleyrat and L. K. Varga, Ferromagnetic Nanocomposites, *Journal of Magnetism and Magnetic Materials*, vv. 215, 2000, pp. 253–259.
- [10]. D. E. Spiliotis, Magnetic Recording beyond the First 100 Years, *Journal of Magnetism and Magnetic Materials*, vv. 93, 1999, pp. 29–35.
- [11]. N. Ikenaga, Y. Ohgaito, H. Matsushima, T. Suzuki, Preparation of zinc ferrite in the presence of carbon material and its application to hot-gas cleaning, *Fuel*, vv. 83, 2004, pp. 661–669.
- [12]. C.W. Jung, P. Jacobs, Physical and chemical properties of superparamagnetic iron oxide MR contrast agents: ferumoxides, ferumoxtran, ferumoxsil, *Magnetic Resonance Imaging*, vv. 13, 1995, pp. 661–674.
- [13]. N.A. Brusentsov, V. Gogosov, et al., Evaluation of ferromagnetic fluids and suspensions for the site-specific radiofrequency-induced hyperthermia of MX11 sarcoma cells invitro, *Journal of Magnetism and Magnetic Materials*, vv. 225, 2001, pp. 113–117.
- [14]. M. Atif, S.K. Hasanain, M. Nadeem, Magnetization of sol-gel prepared zinc ferrite nanoparticles: effects of inversion and particle size, *Solid State Communication*, vv. 138, 2006, pp. 416–421.
- [15]. T. Kamiyama, K. Haneda, T. Sato, S. Ikeda, H. Asano, Cation distribution in ZnFe₂O₄ fine particles studied by neutron powder diffraction, *Solid State Communication*, vv. 81, 1992, pp. 563–566.
- [16]. B. Jayadevan, K. Tohji, K. Nakatsuka, Structure analysis of coprecipitated ZnFe₂O₄ by extended x-ray-absorption fine structure, *Journal of Applied Physics*, vv. 76, 1994, pp. 6325–6327.
- [17]. M. Ebrahimi, R.R. Shahraki, S.A. Seyyed Ebrahimi, S.M. Masoudpanah, Magnetic properties of zinc ferrite nanoparticles synthesized by coprecipitation method, *Journal of Superconductivity and Novel Magnetism*, vv. 27, 2014, pp. 1587–1592.
- [18]. C.N. Chinnasamy, A. Narayanasamy, P. Nagamony, K. Chattopadhyay, H. Guerault, J.M. Greneche, Ferrimagnetic ordering in nanostructured zinc ferrite, *Scripta Materialia*, vv. 44, 2001, pp. 1407–1410.
- [19]. R. RaeisiShahraki, M. Ebrahimi, Structural characterization and magnetic properties of superparamagnetic zinc ferrite nano particles synthesized by the coprecipitation method, *Journal of Magnetism and Magnetic Materials*, vv. 324, 2012, pp. 3762–3765.
- [20]. R. Sai, S.D. Kulkarni, K.J. Vinoy, N. Bhat, S.A. Shivashankar, ZnFe₂O₄: rapid and sub-100 °C synthesis and anneal-tuned magnetic properties, *Journal of Material Chemistry*, vv. 22, 2012, pp. 2149–2156.
- [21]. M. Mozaffari, M. Eghbali Arani, J. Amighian, The effect of cation distribution on magnetization of ZnFe₂O₄ nanoparticles, *Journal of Magnetism and Magnetic Materials*, vv. 322, 2010, pp. 3240–3244.
- [22]. V. Blanco-Gutierrez, E. Climent-Pascual, Neutron diffraction study and superparamagnetic behavior of ZnFe₂O₄ nanoparticles obtained with different conditions, *Journal of Solid State Chemistry*, vv. 184, 2011, pp. 1608–1613.
- [23]. J.L. Xie, M.G. Han, L. Chen, R.X. Kuang, L.J. Deng, Microwave-absorbing properties of NiCoZn spinel ferrites, *Journal of Magnetism and Magnetic Materials* vv. 314, 2007, pp. 37–42.
- [24]. T.J. Shinde, A.B. Gadkari, P.N. Vasambekar, Magnetic properties and cation distribution study of nanocrystalline Ni-Zn ferrites. *Journal of Magnetism and Magnetic Materials*, vv. 333, 2013, pp. 152–155.
- [25]. K. Nejati, R. Zabihi, Preparation and magnetic properties of nano size nickel ferrite particles using hydrothermal method, *Chemistry Central Journal*, vv. 6, 2012, pp. 23–29.
- [26]. M. Kurian. C. Kunjachan, Investigation of size dependency on lattice strain of nanocerium particles

- synthesised by wet chemical methods, *International Nano Letters*, vv. 4, 2014, pp. 73–80.
- [27]. A. Manikandan, J. Judith Vijaya, M. Sundararajan, C. Meganathan, L.J. Kennedy, M. Bououdina, Optical and magnetic properties of Mg-doped ZnFe_2O_4 nanoparticles prepared by rapid microwave combustion method, *Superlattices and Microstructures*, vv. 64, 2013, pp. 118–131.
- [28]. R.P. Patil, S.D. Delekar, D.R. Mane, P.P. Hankare, Synthesis, structural and magnetic properties of different metal ion substituted nanocrystalline zinc ferrite, *Results in Physics*, vv. 3, 2013, pp. 129–133.
- [29]. S.S. More, R.H. Kadam, A.B. Kadam, D.R. Mane, G.K. Bichile, Structural properties and magnetic interactions in Al^{3+} and Cr^{3+} co-substituted CoFe_2O_4 ferrite, *Central European Journal of Chemistry*, vv. 8, 2010, pp. 419–425.
- [30]. W. Konicki, D. Sibera, E. Mijowska, Z.L. Bielun, U. Narkiewicz, Equilibrium and kinetic studies on acid dye Acid Red 88 adsorption by magnetic ZnFe_2O_4 spinel ferrite nanoparticles, *Journal of Colloid and Interface Science*, vv. 398, 2013, pp. 152–160.
- [31]. R. D. Waldron, Infrared spectra of ferrites, *Physical Review Journal*, vv. 99, 1955, pp. 1727.
- [32]. S.A.V. Prasad, M. Deepty, P.N. Ramesh, G. Prasad, K. Srinivasarao, Ch. Srinivas, K. Vijaya Babu, E.R. Kumar, N.K. Mohane, D.L. Sastry, Synthesis of MFe_2O_4 ($\text{M} = \text{Mg}^{2+}, \text{Zn}^{2+}, \text{Mn}^{2+}$) spinel ferrites and their structural, elastic and electron magnetic resonance properties, *Ceramics International*, vv. 44, 2018, pp. 10517–10524.
- [33]. S. S. Shinde, Crystal Structure and Magnetic Interactions of Ferrites, *International Journal of science and research*, vv. 5, 2016, pp. 2015–2017.
- [34]. B.D. Cullity and C.D. Graham, *Introduction to Magnetic Materials*, (2009) 2nd edition (Wiley, Hoboken, NJ).